Journal of Sound and Vibration (2000) **235**(1), 117–132
doi:10.1006/jsvi.2000.2914, available online at http://www.idealibrary.com on IDEAL®

FREE VIBRATION OF COUPLED DISK–HAT STRUCTURES

J. C. BAE

North American Automotive Group, General Motors Corporation, Warren, MI, U.S.A.

AND

J. A. WICKERT

Department of Mechanical Engineering, Carnegie Mellon University, Pittsburgh, PA 15213-3890, *U.S.A.*

(*Received* 3 *May* 1999, *and in final form* 24 *January* 2000)

The free vibration of disk–hat structures, such as automotive brake rotors, is investigated analytically and through laboratory experimentation. Of particular interest are the role played by the hat element's depth in influencing the three-dimensional vibration of the disk, and the manner in which the bending and in-plane modes of the disk alone evolve as a hat of increasing depth is incorporated in the model. The lower vibration modes of disk–hat structures are shown to be characterized by the numbers of nodal circles *NC* and diameters *ND* present on the disk, as well as the phase relationship between the disk's transverse and radial displacements due to coupling with the hat element. Such modes map continuously back to the pure bending and in-plane modes of the disk alone, appear in ordered pairs, and can exist at close frequencies. Those characteristics are explored particularly with respect to sensitivities in the disk's thickness and the hat's depth with a view towards shifting particular natural frequencies, or minimizing transverse disk motion in certain vibration modes. Results obtained through analysis and measurement of a prototypical disk–hat structure are applied in a case study with a ventilated automotive brake rotor.

1. INTRODUCTION

Unwanted noise and vibration associated with the braking process in passenger automobiles has become an important economic and technological problem in the industry, and one that encompasses a broad range of disciplines including mechanical vibration, acoustics, friction, materials, and interface chemistry. Disk brake noise and vibration are known to involve structural coupling between such components as the rotor, pads, caliper, and knuckle. Further, depending on the frequency range of interest, the hydraulic system, body panels, steering column, and other vehicle components can also become active. In an aggregate sense, the disk brakes of only a few percent of new vehicles exhibit sufficient noise and vibration to generate significant customer complaints, but the volume and expense of remediation efforts, in addition to the perception of reduced product-line quality, place pressure on brake noise and vibration engineering efforts.

An acute problem is the so-called "squeal" noise, which is typically defined as that occurring within the range 1·5–20 kHz at one or more of the rotor's natural frequencies and its harmonics. As depicted n Figure 1 for ventilated and solid core designs, rotors have the distinction of being structural elements, members of the disk–pad friction pair, and efficient radiators of sound because of their large surface area. In each case, the rotor comprises the

0022-460X/00/310117 + 16 $35.00/0

(a)

(b)

(c)

Figure 1. Photographs of typical (a) shallow-hat ventilated, (b) deep-hat ventilated, and (c) solid core brake rotors having different disk and hat element dimensions.

"disk" element which is in frictional contact with the pads during operation, and the "hat" element which provides the geometric offset necessary for mounting the rotor to the vehicle. The thickness, inner diameter (I.D.) and outer diameter (O.D.) of the disk; the depth and thickness of the hat; and the numbers and spacings of the cooling vanes and mounting studs are some of the geometric parameters that set the rotor's natural frequency spectrum and vibration modes. Improved understanding of disk–hat structural vibration offers one opportunity for targeted improvements in brake rotor design.

By way of background, in the case of an idealized annular disk without a hat element, the lower frequency vibration modes fall into two distinct classes: the bending B (transverse) and in-plane IP (radial–circumferential) modes which are further classified according to the numbers of nodal circles NC and diameters ND present. Figure 2 depicts variation of the

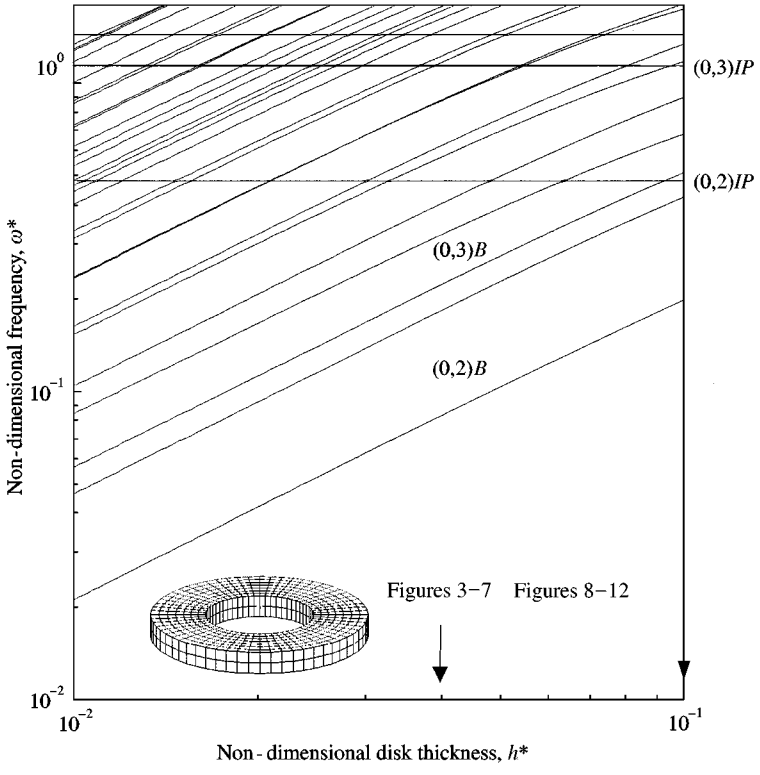

Figure 2. Natural frequency spectrum for the three-dimensional vibration of a free annular disk as a function of its thickness; $a^* = 0{\cdot}5$. Over this range of h^*, the frequencies of the bending modes B increase with thickness, while those of the in-plane modes IP are insensitive to it.

non-dimensionalized B and IP natural frequencies as functions of dimensionless disk thickness h^*, defined as the ratio of the disk's physical thickness h to its outer diameter b. Here and in what follows, the physical circular frequency ω is non-dimensionalized as ω^* with respect to the material's compression wave speed according to $\omega^* = \omega\sqrt{\rho b^2/4(\lambda + 2\mu)}$, where ρ denotes the volumetric density, and λ and μ are Lamé constants. The calculation is based on an analysis of the governing equations for three-dimensional vibration of a disk having arbitrary thickness [1]. As expected on the basis of plate theory, the natural frequencies of the bending modes increase in a substantially linear manner with h^* over the depicted range of thickness. The frequencies of the in-plane modes, on the other hand, are largely insensitive to h^* over this range.

For illustration, the $(0, 2)B$ and $(0, 2)IP$ modes are shown in Figure 3. The manner in which those and other bending and in-plane modes change as the hat element is incorporated in the model, and the degree to which variations in the natural frequencies and mode shapes can be used to advantage in designing rotors, form emphases of this study. Of particular interest is the continuous transition from disk-like behavior (in which case the vibration modes are readily classified as being either bending or in-plane) to coupled–hat system behavior (where the modes are fully three-dimensional but retain certain characteristics of the generating B and IP classes).

Literature related to the free vibration of related but different structures includes treatments of the bending of annular plates having moderate thickness [1–3], and the three-dimensional motion of solid [4], hollow [5], or arbitrarily shaped [6] cylinders. Also

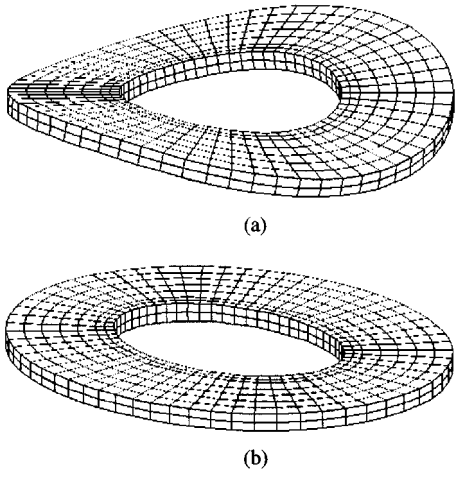

Figure 3. Two nodal diameter disk (a) bending and (b) in-plane modes; $h^* = 0{\cdot}04$.

relevant to the present investigation is the vibration of combined plate and cylindrical shell structures, for instance, where one end of the shell is capped by a circular plate while the other remains open [7] or where both ends are closed [8]. With regard to the latter, both substructuring techniques and finite element analyses have been used to predict the natural frequencies [9]. An alternative approach based upon the Rayleigh–Ritz method, in which the shell and plate components are joined through the use of artificial springs to facilitate the selection of expansion functions, is discussed in reference [10]. The case of boundary conditions modelled through elastic restraints has been examined in the context of such combined plate–shell systems wherein the structure's modes were categorized as being plate-controlled, shell-controlled, or strongly coupled [11].

In what follows, a prototypical model of a disk–hat structure is examined in which vibration of the disk couples with an open cylindrical hat element attached at the disk's inner periphery. This structure is represented as a reduced-order model of a brake rotor to the extent that the hat affords impedance coupling to the disk along its inner boundary. The variation in frequency and shape of the vibration modes, beginning at the limiting condition of a disk alone having moderate thickness, is examined as the hat element is first incorporated, and then as its depth is subsequently increased. In the presence of the hat element, the bending and in-plane modes of the disk alone are shown to transition into companion members of pairs denoted $(NC, ND)\pm$, for which the magnitudes of the disk's transverse displacement can be the same, different, or zero depending on the hat's depth.

2. DISK–HAT STRUCTURE MODEL

Figure 4 illustrates the prototypical disk–hat structure used for investigating the transition of the disk's bending and in-plane modes in the presence of an integral hat element. The structure is axisymmetric and formed of an isotropic homogeneous elastic material, and all surfaces are specified to be traction-free. Four dimensional parameters—a, b, d, and h—represent the disk's inner and outer diameters, the hat depth, and the common disk and hat wall thickness respectively. All lengths here and in what follows are non-dimensionalized with respect to b and are henceforth denoted by variables having an asterisk superscript. For instance, over a representative sampling of eight-brake

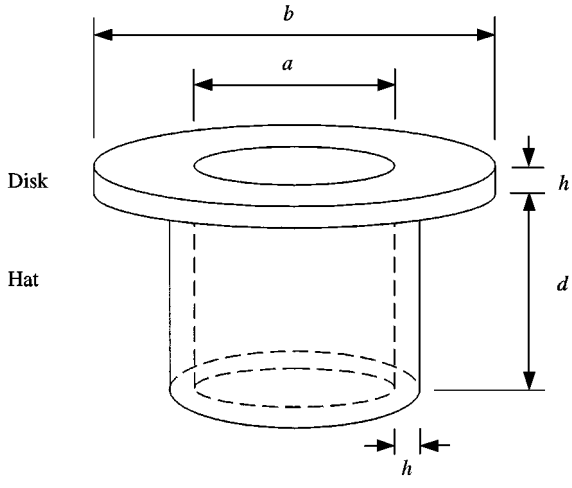

Figure 4. Schematic of a prototypical, free, annular, axisymmetric disk–hat structure.

rotor designs, typical parameter values fall in the ranges $0{\cdot}5 < a^* < 0{\cdot}7$, $0{\cdot}05 < d^* < 0{\cdot}20$, and $0{\cdot}04 < h^* < 0{\cdot}10$.

The natural frequencies and modes of the disk–hat model were determined through finite element discretization. The mesh was refined as necessary to produce results which converged to four significant digits over the discussed range of d^*. The structure was represented by solid brick elements having eight nodes, each with six degrees of freedom in translation and rotation. Over the disk, seven elements were allocated in the radial direction, and 60 in the circumferential direction. Over the depth of the hat, one element was added for each increment of 0·04 in d^*.

Laboratory tests were also conducted on solid disk–hat structures that were machined of aluminum ($a = 76$ mm, $b = 152$ mm, and $h = 6$ mm), and the natural frequencies were identified for 13 different values of hat depth between 0 and 76 mm. The structures, supported only on compliant foam, were excited impulsively by a hammer instrumented with a piezoelectric force sensor; displacement and force time records were recorded; and a spectrum analyzer characterized the signals in the frequency domain. Peaks in the measured transfer functions provided the natural frequencies. By transferring an ensemble of measurements to an available data acquisition computer, vibration modes were determined through standard techniques of experimental modal analysis.

3. NATURAL FREQUENCY AND MODE STRUCTURE

Values $a^* = 0{\cdot}5$, and $h^* = 0{\cdot}04$ or 0·1, were used in case studies investigating the variation of natural frequencies and modes over hat depths $0{\cdot}0 < d^* < 0{\cdot}5$. For the case $h^* = 0{\cdot}04$, Figure 5 depicts changes in the predicted (solid lines) and measured (points) natural frequencies; those values agree in the aggregate within 4% over the full d^* range. At $d^* = 0$, the values for the lower bending and in-plane frequencies of a moderately thick annular disk are recovered [1, 3]. As deduced from Figure 2, at $d^* = 0$ in Figure 5 the first five modes $(0, 2)B$, $(1, 0)B$, $(1, 3)B$, $(1, 1)B$ and $(0, 4)B$ are of the bending class, while the sixth mode $(0, 2)IP$ is the fundamental in-plane mode. Beginning with the bending and in-plane modes of the disk alone at $d^* = 0$, the loci are extended in Figure 5 for the modes $(0, ND)$ with $2 < ND \leqslant 5$, and $(1, ND)$ with $0 < ND \leqslant 3$.

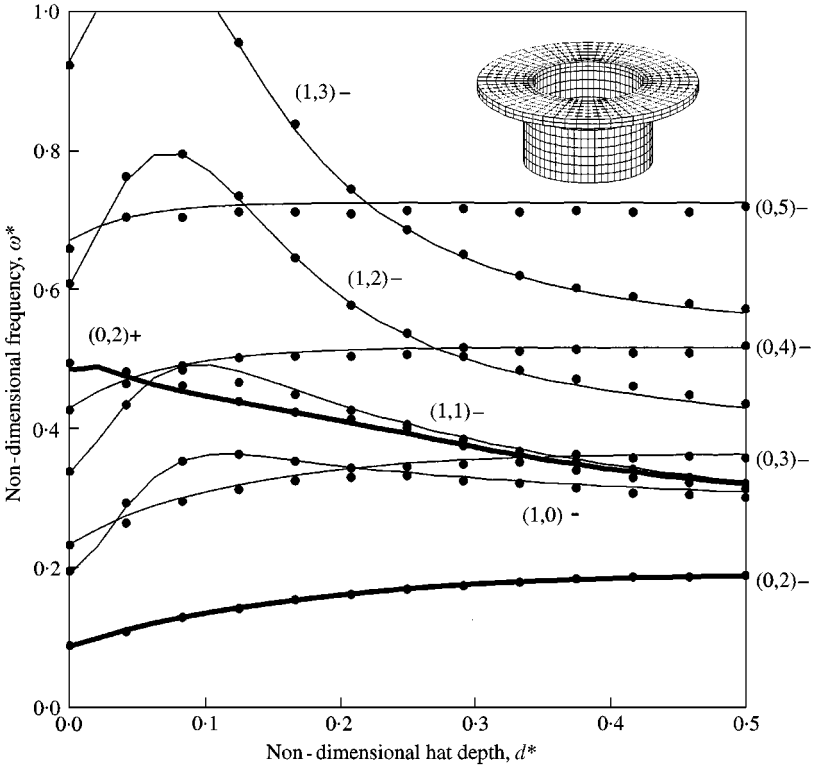

Figure 5. Natural frequency spectrum for the three-dimensional vibration of a disk–hat structure as a function of hat depth; $h^* = 0{\cdot}04$ and $a^* = 0{\cdot}5$. Loci for the (0, 2) $\pm$ pair of modes are highlighted. (——), model predictions (●), measurements.

As the hat's depth grows, the natural frequencies and mode shapes undergo continuous transition from those of a disk alone to those of a coupled disk–hat structure. Whereas the lower modes of the disk alone are readily classified as being members of either the B or IP classes, such a representation is not appropriate for disk–hat structures to the degree that their modes involve coupled transverse and in-plane displacement components. For instance, in treating the vibration of shell–plate structures, references [9, 10] classified modes according to their symmetry, while in reference [11], a convention was adopted based on whether motions of the shell or plate were judged to be dominant. In the present application, each vibration mode of the disk–hat structure maps continuously in the limit of vanishing d^* to either a bending or in-plane mode of the disk alone having designation (NC, ND). By convention, those modes that transition to a (lower frequency) bending mode of the disk alone are denoted $(NC, ND) -$, while those tending toward the companion (higher frequency) in-plane mode are denoted $(NC, ND) +$. In addition to identifying the relative frequencies of the mode pair, the "$\pm$" suffix also differentiates the phase relationship between transverse vibration of the disk and radial vibration of the hat element. Pairs of companion modes having different frequencies have also been discussed within the context of hollow cylinders and shell–plate structures [6, 7].

The natural frequencies for members of the $(0, ND) -$ class of modes grow moderately with increasing depth over the range considered in Figure 5. Members of the $(1, ND) -$ class have frequencies which do not behave monotonically but are generally maximized

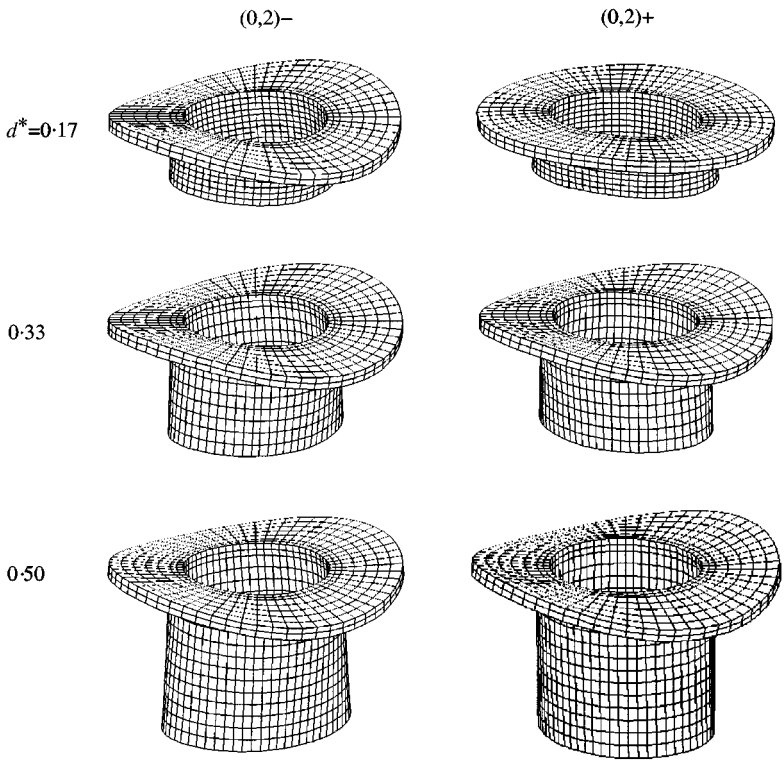

Figure 6. Evolution of the (0, 2) $\pm$ mode shapes as sampled along their frequency loci in Figure 5.

near $d^* \approx 0{\cdot}1$ for the lower modes. A hat depth near that value could be considered optimal, for instance, in the sense that those modes are stiffened.

The locus for the (0, 2) + mode generally decreases in Figure 5, and changes in sequence from the sixth mode at $d^* = 0$ to the third at $d^* = 0{\cdot}35$. In short, the mode sequence shifts with hat depth with loci for the " $\pm$ " pair of modes generally approaching one another. The transition, or "morphing", of the (0, 2) $\pm$ mode shapes is illustrated in Figures 3 (at $d^* = 0$) and 6 (at $d^* = 0{\cdot}17$, 0·33, and 0·50). At $d^* = 0$, the (0, 2) $\pm$ pair reduces to the two nodal diameter bending and in-plane modes of an idealized disk, but with increasing d^*, the modes transition to become generally three dimensional in character. In fact, from the standpoint of measurements mode on the disk alone, and with respect only to the specification of *NC* and *ND* for the disk's transverse motion, those modes are not easily distinguished at $d^* = 0{\cdot}33$ and 0·5 to the degree that both the (0, 2) − and (0, 2) + modes have decidedly bending-like appearances with substantially similar displacements over the surface of the disk itself. Transverse motion of the disk dominates the displacement field of the (0, 2) + mode at a frequency near that of (0, 2) − for substantial hat depths, notwithstanding its genesis as an in-plane mode of the disk alone.

A further distinction between the (0, 2) $\pm$ modes is seen in Figure 7, where they are shown at $d^* = 0{\cdot}33$ in both isometric and section views. In the case of (0, 2) − , transverse deformation of the disk and radial displacement of the hat occur in-phase, and precisely the opposite is true for (0, 2) + . A cross-section of the disk rotates in (0, 2) − with respect to the point of connection between the disk and hat elements, with motion of the two elements occurring in the same direction. The cross-section shown in Figure 7 (0, 2) + , on the other hand, exhibits both radial translation of the connection point and rotation about it.

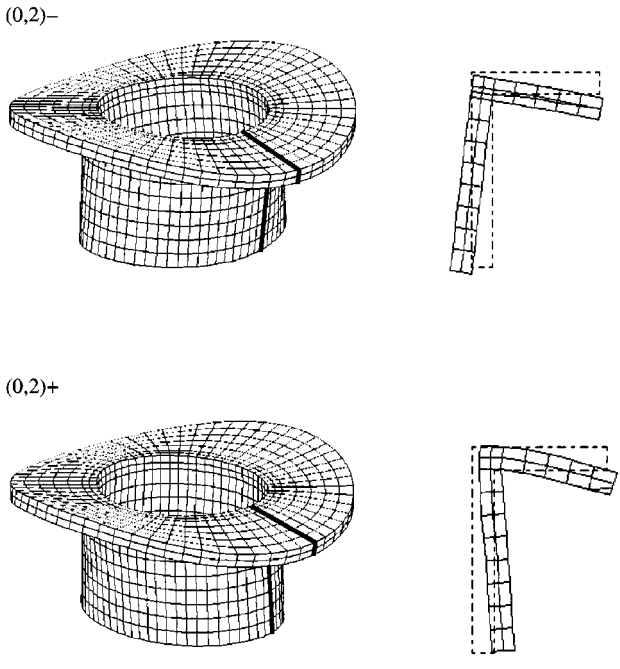

Figure 7. Isometric and cross-sectional views of the (0, 2) $\pm$ modes at $d^* = 0{\cdot}33$, depicting similar transverse displacements over the disk but differing phase relationships between the disk and hat elements. The section is taken along an antinode of the disk's transverse displacement.

4. BENDING AND IN-PLANE DISPLACEMENT COMPONENTS

When the common disk and hat thickness is increased to $h^* = 0{\cdot}1$, loci for the (0, 2) $\pm$ and (0, 3) $\pm$ pairs of modes approach at values $d^* \approx 0{\cdot}3$ and $0{\cdot}5$, respectively, as indicated in Figure 8. Frequencies of the individual (0, 2) $\pm$ and (0, 3) $\pm$ pairs remain distinct, however, for large d^* owing to differences in strain energy, behavior also observed in companion hollow cylinder [6] and shell–plate [7] structures. At higher frequencies not shown in Figure 8, the loci of (0, 4) $\pm$, (0, 5) $\pm$, and higher ND pairs also approach one another. In a different process, the loci for the $(1, ND)-$ family, with $ND = 0, 1, 2, \ldots$, exhibit coalescence at hat depth values above $0{\cdot}5$ in a manner analogous to the development of frequency clusters in the vibration of long cylinders [12].

Several plan views of the (0, 3) $\pm$ modes are shown in Figure 9. At $d^* = 0$, the (0, 3) $\pm$ modes have qualitatively distinct appearances, but those differences diminish as the hat with finite depth is introduced. At $d^* = 0{\cdot}5$, for instance, the disk elements alone in both the $(0, 3)-$ and $(0, 3)+$ modes have sensibly similar shapes. A distinction between these modes, however, is the different phase relationship between the disk's transverse motion and the hat's radial motion at larger d^* values. At $d^* = 0{\cdot}5$, the disk's (upward) transverse displacement and the hat's (outward) radial displacement in $(0, 3)-$ occur with the same phase, but those displacements are out-of-phase in the slightly higher frequency (0, 3) $\pm$ mode. As for (0, 3) $\pm$ here and (0, 2) $\pm$ in Figure 6, such modes are each dominated by transverse deformation of the disk, notwithstanding the continuous mapping of $(0, 3)+$ and $(0, 2)+$ back to pure in-plane modes of an annular disk alone.

Specifically, Figures 10 and 11 quantify transition of the transverse (u_z) and combined radial (u_r) and circumferential (u_θ) displacements for the (0, 2) $\pm$ and (0, 3) $\pm$ modes, as

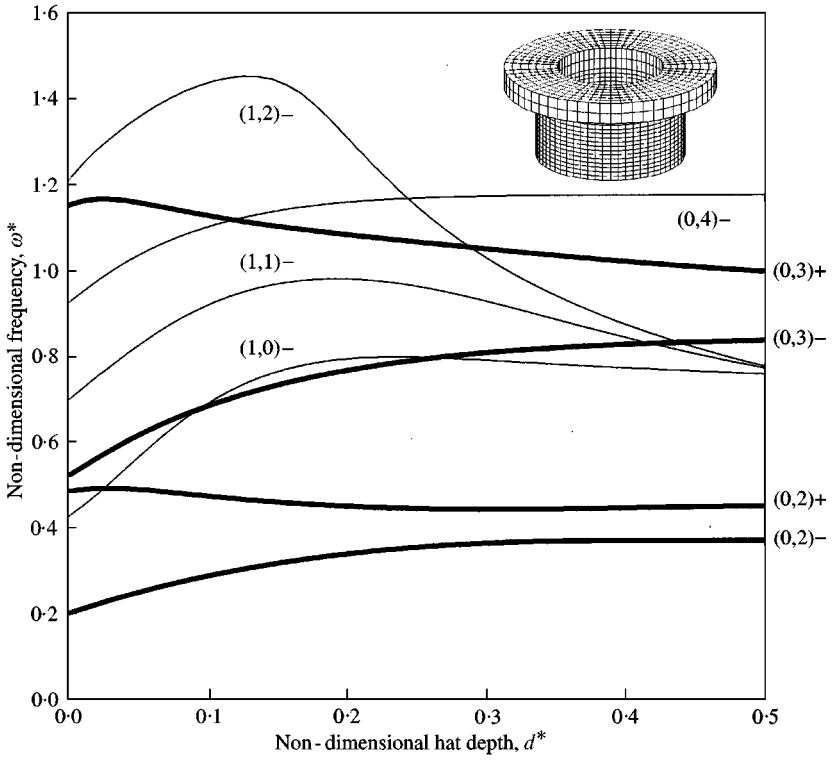

Figure 8. Natural frequency spectrum for the three-dimensional vibration of a disk–hat structure as a function of hat depth; $h^* = 0{\cdot}1$ and $a^* = 0{\cdot}5$. Loci for the (0, 2) $\pm$ and (0, 3) $\pm$ pairs of modes are highlighted.

taken at the disk's midplane around its outer periphery. The displacement components of those modes have dependencies $u_r = A_r \cos(ND\,\theta)$, $u_\theta = A_\theta \sin(ND\,\theta)$, and $u_z = A_z \cos(ND\,\theta)$ [7]. Beginning in Figure 10 with (0, 2) $-$, the mode shape is normalized at each d^* such that the peak value of the out-of-plane displacement is unity, namely $|A_z| = 1$. That component is used as the point of reference since (0, 2) $-$ transitions to a bending mode of the disk alone. The magnitude of combined u_r and u_θ motions, on the other hand, is measured by $\sqrt{A_r^2 + A_\theta^2}$, which is proportional by the factor $\sqrt{2}$ to the root-mean-square average of in-plane displacement. The in-plane displacement norm grows from zero at $d^* = 0$ to the maximum of 0·17 at $d^* \approx 0{\cdot}2$ before decreasing for larger values of d^*. Thus, the bending mode of the disk, following introduction of the hat, evolves into a three-dimensional shape in which the transverse displacement of the disk continues to dominate the in-plane displacement by a factor of at least 5 : 1 throughout the entire range of hat depths examined.

A rather different situation develops for the companion (0, 2) $+$ mode as depicted in the lower element of Figure 10. Since this mode maps to a pure in-plane mode of the disk alone, $|A_z|$ is compared to $\sqrt{A_r^2 + A_\theta^2}$ by alternatively scaling the in-plane displacement norm to unity. At $d^* = 0$, the transverse displacement begins from zero, reaches the local maximum of 0·26 at $d^* = 0{\cdot}08$, passes through zero at $d^* = 0{\cdot}186$, and rises to the value 0·90 at $d^* = 0{\cdot}5$. The cusp-like behavior at $d^* = 0{\cdot}186$ represents an A_z zero crossing and is an artifact of the absolute value operation. At $d^* = 0{\cdot}08$, for instance, the in-plane displacements dominate the transverse motion by a factor of 4 : 1. However, for values of hat depth

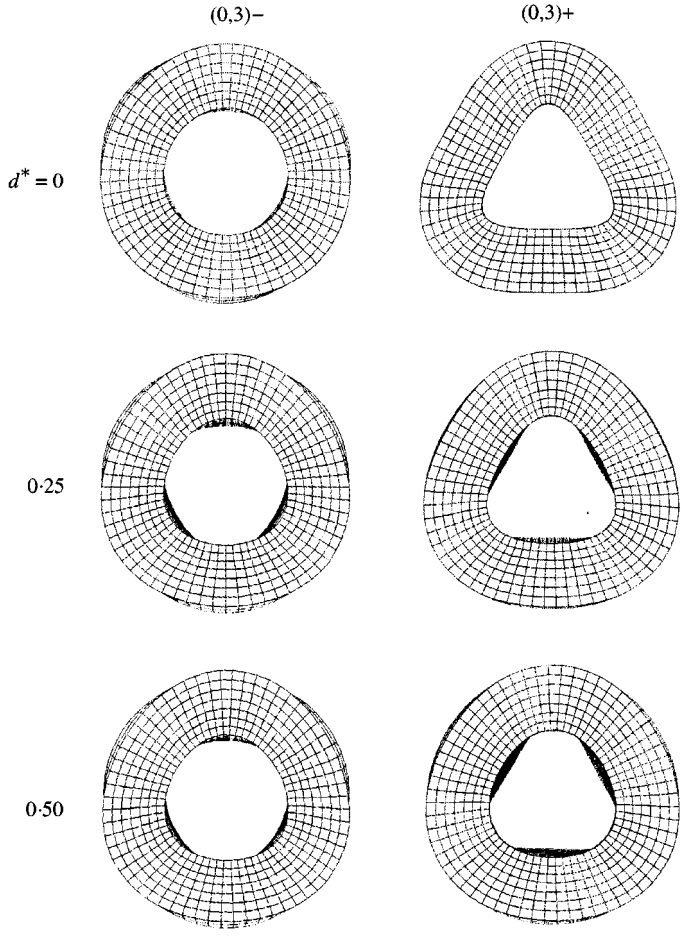

Figure 9. Evolution of the (0, 3) $\pm$ mode shapes as sampled along their loci in Figure 8. The differing phase relationships between the disk and hat are evident in the views at $d^* = 0{\cdot}25$ and 0·5.

greater than $d^* \approx 0{\cdot}35$, the transverse displacement has grown to become substantially similar in magnitude to that of the in-plane displacements. In fact, at $d^* = 0{\cdot}5$, the in-plane displacement magnitude is some 90% of the transverse magnitude. Thus, the (0, 2) + mode is no longer fairly described as being "in-plane", and from the standpoint of a vibration measurement performed on the disk itself of the disk–hat structure (as is conventional) twin two-nodal diameter modes separated by some 18% in frequency would appear to be present, even for this axisymmetric model.

Figure 11 presents analogous results for the (0, 3) $\pm$ pair. Transverse displacement dominates in-plane motion of (0, 3) − by a factor of some 7 : 1 over the entire d^* range. For (0, 3) +, on the other hand, although $|A_z|$ has a local maximum at $d^* = 0{\cdot}063$, $|A_z|$ and $\sqrt{A_r^2 + A_\theta^2}$ grow to become identical (unity) at $d^* = 0{\cdot}370$. Further, the transverse displacement vanishes at $d^* = 0{\cdot}168$, a value which is pleasingly near the corresponding point where $|A_z| = 0$ for (0, 2) + in Figure 10. Both zero crossing values fall within the range of d^* that is judged to be practical from the standpoint of typical rotor design. Transition of the (0, 3) + mode is depicted in the sequence of Figure 12, where the shapes are sampled at the hat depths indicated by the bold data points in Figure 11. In both Figures 10 and 11,

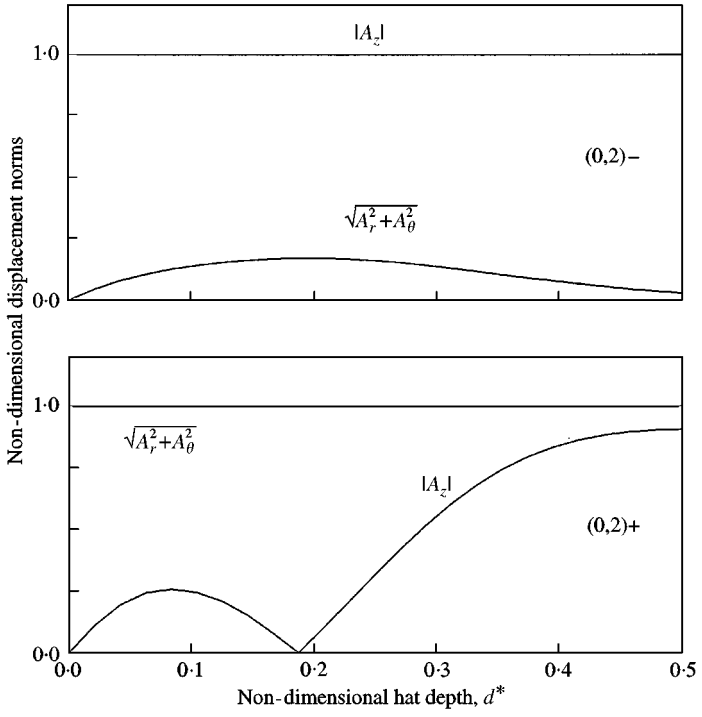

Figure 10. Norms of the disk's displacement components for the (0, 2) $\pm$ pair of modes as a function of hat depth; $h^* = 0{\cdot}1$ and $a^* = 0{\cdot}5$.

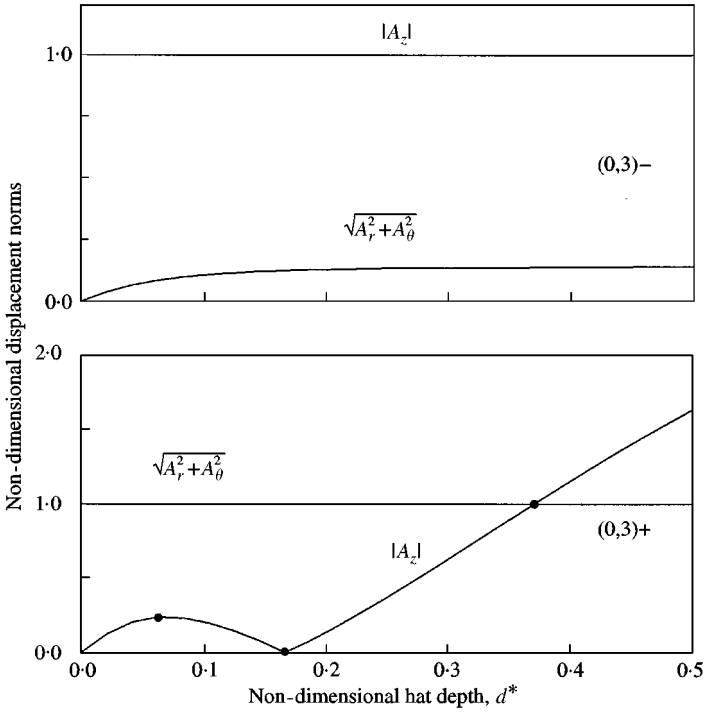

Figure 11. Norms of the disk's displacement components for the (0, 3) $\pm$ pair of modes as a function of hat depth; $h^* = 0{\cdot}1$ and $a^* = 0{\cdot}5$. Mode shapes sampled at the highlighted points are illustrated in Figure 12.

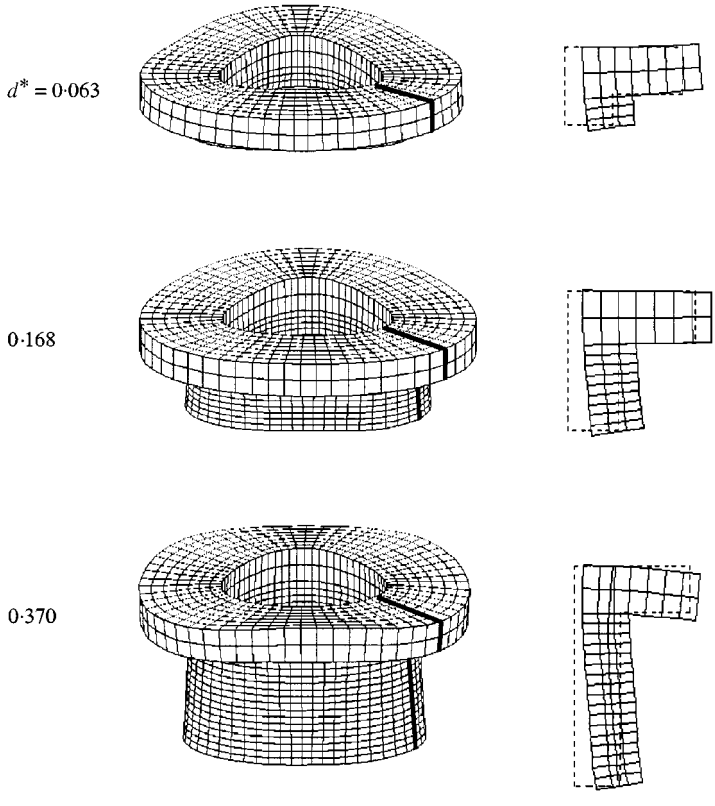

Figure 12. Isometric and section views of the (0, 3) + mode sampled at the hat depths indicated in Figure 11 in order to demonstrate in-phase disk transverse and hat radial motions at $d^* = 0{\cdot}063$, vanishing transverse displacement at $d^* = 0{\cdot}168$, and out-of-phase disk transverse and hat radial motions at $d^* = 0{\cdot}370$.

there is no zero (or sign change) in the transverse displacement component, relative to that of the in-plane component, for either (0, 2) − or (0, 3) − . That is, both modes retain the same phase relationship between u_z and u_r over the full range of d^* as depicted in, for instance, the cross-sectional view of Figure 7. On the other hand, zero crossings do occur for (0, 2) + and (0, 3) + , a situation which also appears to be the case for other (NC, ND) + modes that have been examined.

5. BRAKE ROTOR APPLICATION

A parameter study in hat depth is used to illustrate application of the findings to the vibration analysis of brake rotors using the uppermost rotor shown in Figure 1 as the benchmark design. Figure 13 depicts a collocated point transfer function of the rotor as measured in the transverse direction on the outer periphery of the disk. The spectral peaks for the (0, 2) $\pm$ modes are labelled, where those modes were identified using standard techniques of experimental modal analysis with an impact hammer and a triaxial accelerometer. Other peaks shown correspond to modes having different NC and ND over the surface of the disk, but the salient point here is the presence of two modes, as identified through transverse vibration measurement, having essentially identical nodal patterns on the surface of the disk.

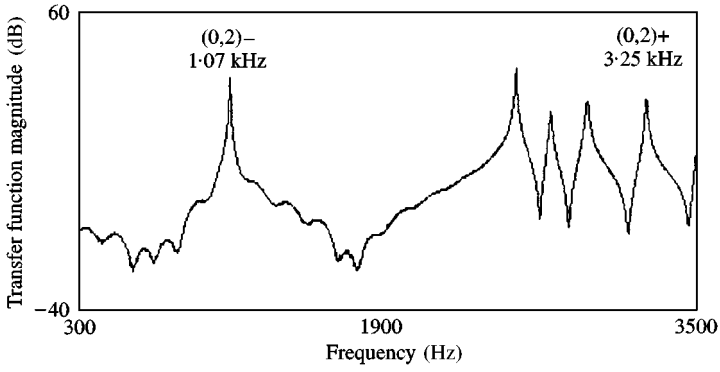

Figure 13. Collocated point transfer function of the uppermost rotor shown in Figure 1, as measured at the disk's outer pariphery in the transverse direction.

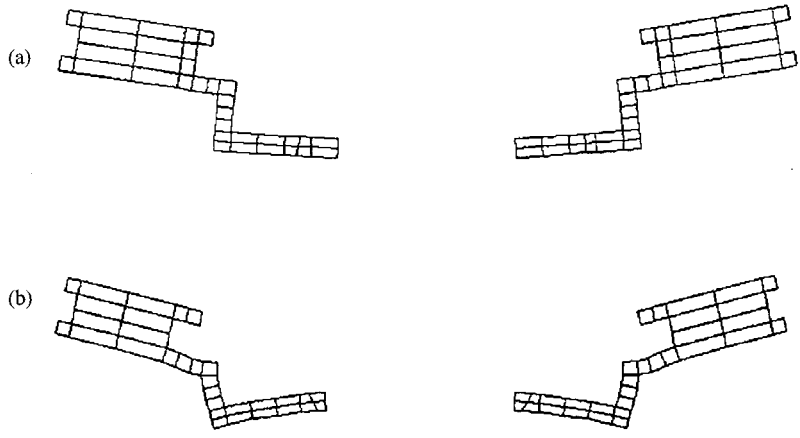

Figure 14. Section views of the rotor's predicted (a) (0, 2) − and (b) (0, 2) + modes.

A finite element model of the rotor accounted for the geometry of the inner and outer disks, the pattern of cooling fins between the disks, and the hat structure. The overall dimensions of the rotor were $a = 129$ mm, $b = 245$ mm, and $h = 18$ mm. By using the value 3540 m/s for the compression wave speed in cast iron, as determined through a least-squares fit of the model to the frequency measurements over a 6·4 kHz bandwidth, the rotor model predicted frequencies 1·07 and 3·17 kHz ((0, 2) $\pm$), and 2·68 and 5·36 kHz ((0, 3) $\pm$).

Figure 14 depicts through cross-section views the predicted phase relationships between u_r and u_z in the (0, 2) $\pm$ modes, analogous to the results of Figure 7 for the prototypical disk–hat model. The radial and transverse displacements as developed around the disk's outer periphery were measured for the (0, 2) $\pm$ pair of modes, with results shown in Figure 15. Although these modes differ in frequency by some 2·18 kHz, they each contain two nodal diameters and no nodal circles over the disk's surface, and have significant transverse motion relative to in-plane displacement. In Figure 15, the modal amplitudes are normalized with respect to the maximum value (unity) of u_z. The radial displacement for (0, 2) + is slightly larger than that for its companion (0, 2) − to the extent that the former evolved from an in-plane mode. For this benchmark case at least, the distinction between the rotor's two nodal diameter "bending" and "in-plane" modes blurs, with comparable

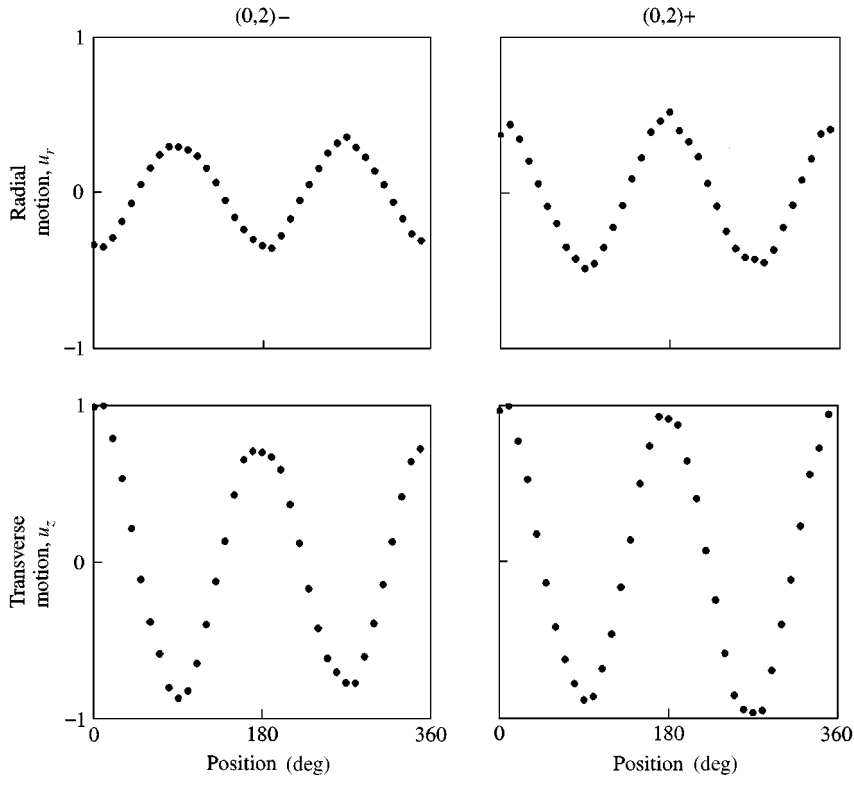

Figure 15. Measurements of the brake rotor's radial and transverse displacement components in the (0, 2) $\pm$ modes at 1·07 and 3·25 kHz, respectively, as taken around the disk's outer periphery.

magnitude displacements occurring in the transverse and radial directions, but with opposite phase, for each.

Figure 16 shows the predicted natural frequencies of the rotor as a function of hat depth, with 18 mm being the rotor's design point. The natural frequencies for the (0, 2) $\pm$ and (0, 3) $\pm$ modes vary in a manner analogous to that seen in Figures 5 and 8. The natural frequency for a member of the (0, *ND*) $-$ class of modes grows moderately, while that for each (0, *ND*) $+$ mode decreases, with increasing hat depth.

6. SUMMARY

In this investigation, the role played by a hat element in evolving the in-plane and transverse modes of an idealized disk of moderate thickness into fully three-dimensional modes, which present significantly coupled motions in the in-plane and transverse directions, is examined. In particular, transition of the bending and in-plane modes of the disk alone into coupled (*NC*, *ND*) $\pm$ pairs is emphasized, in which case the magnitudes of the disk's transverse displacement in the companion modes can be the same, different, or zero depending on the value taken by the hat's design parameter d^*. Other design parameters, such as the hat's wall thickness, could offer similar behavior and design flexibility.

Vibration of brake rotors is conventionally described in terms of motion of the disk alone by specifying the number of nodal diameters and circles present in the transverse

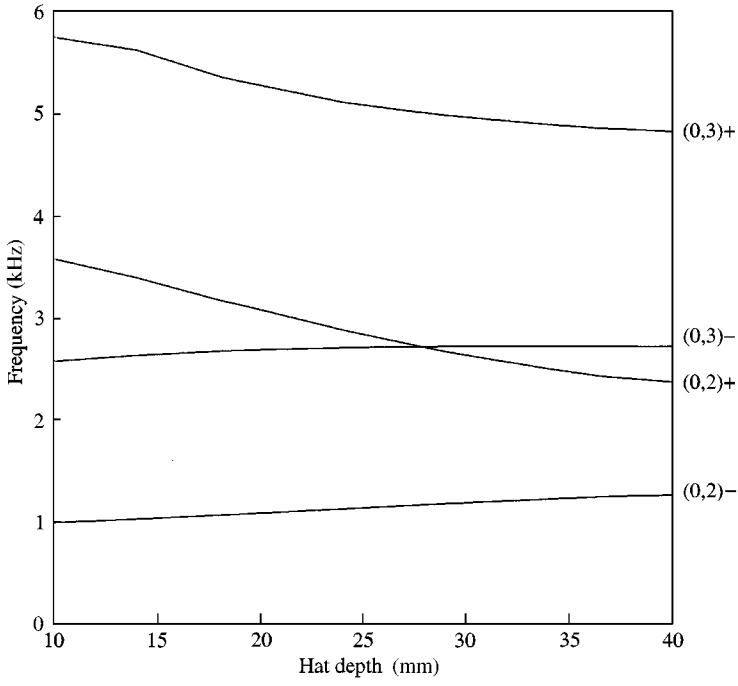

Figure 16. Predicted variation of the rotor's natural frequencies in the (0, 2) $\pm$ and (0, 3) $\pm$ pairs of modes as a function of hat depth.

deformation of the disk itself. That description is not preferred to the degree that mode pairs $(NC, ND) \pm$ exist, each potentially having significant transverse displacement and differing frequencies which can fall in the same general range. Measurements and parameter studies performed on a benchmark ventilated rotor demonstrate in application the presence of a pair of modes having the same number of nodal diameters and circles on the disk (which are emphasized in the brake noise and vibration community) but different frequency and phase coupling with the hat (which are not).

In the case studies evaluated here, disk–hat structures having deep hats have as one characteristic the property that the transverse displacements for the $(NC, ND) +$ modes can be of the same magnitude as the in-plane displacements themselves. Such modes are judged to be excited by in-plane forces, such as frictional loading, and capable of responding with transverse vibration of the disk, with vibration and noise radiation occurring subsequently. Conversely, certain values of hat depth exist at which the transverse displacement component of the $(NC, ND) +$ modes vanishes, a design point which is viewed as desirable to the extent that even in the presence of significant excitation of such modes, the disk would not respond in the transverse direction. Although many mechanisms are thought to be responsible for the coupling process between in-plane and transverse motions of the disk, including normal load variations and caliper or pad dynamics, out-of-plane motion occurring in certain disk modes in judged to be one contributing factor. Designs at critical values of d^* can avoid transverse displacements being present for certain modes.

ACKNOWLEDGMENT

This work was supported by the National Science Foundation and the authors' group of industrial partners.

REFERENCES

1. K. I. TZOU, J. A. WICKERT and A. AKAY 1998a *ASME Journal of Vibration and Acoustics* **120**, 384–391. In-plane vibration modes of arbitrarily thick disks.
2. S. S. RAO and A. S. PRASAD 1975 *Journal of Sound and Vibration* **42**, 305–324. Vibrations of annular plates including the effects of rotatory inertia and transverse shear deformation.
3. J. R. HUTCHINSON 1984 *ASME Journal of Applied Mechanics* **51**, 581–585. Vibrations of thick free circular plates, exact versus approximate solutions.
4. A. W. LEISSA and J. SO 1995 *Journal of the Acoustical Society of America* **98**, 2136–2141. Accurate vibration frequencies of circular cylinders from three-dimensional analysis.
5. J. SO and A. W. LEISSA 1997 *ASME Journal of Vibration and Acoustics* **119**, 89–95. Free vibrations of thick hollow circular cylinders from three-dimensional analysis.
6. K. M. LIEW, K. C. HUNG and M. K. LIM 1995 *ASME Journal of Applied Mechanics* **62**, 718–724. Vibration of stress-free hollow cylinders of arbitrary cross section.
7. B. L. SMITH and E. E. HAFT 1967 *AIAA Journal* **5**, 2080–2082. Vibration of a circular cylindrical shell closed by an elastic plate.
8. S. TAKAHASHI and Y. HIRANO 1970 *Bulletin of the JSME* **13**, 240–247. Vibration of a combination of circular plates and cylindrical shells. (First report: a cylindrical shell with circular plates at ends.)
9. M. S. TAVAKOLI and R. SINGH 1990 *Journal of Sound and Vibration* **136**, 141–145. Modal analysis of a hermetic can.
10. J. YUAN and S. M. DICKINSON 1994 *Journal of Sound and Vibration* **175**, 241–263. The free vibration of circularly cylindrical shell and plate systems.
11. L. CHENG and J. NICOLAS 1992 *Journal of Sound and Vibration* **155**, 231–247. Free vibration analysis of a cylindrical shell-circular plate system with general coupling and various boundary conditions.
12. K. I. TZOU, J. A. WICKERT and A. AKAY 1998b *ASME Journal of Applied Mechanics* **65**, 797–803. Frequency clusters in the spectrum of annular cylinders.